SCIENTIFIC REPORTS

OPEN

Effect of annealing on a pseudogap state in untwinned $YBa_2Cu_3O_{7-\delta}$ single crystals

A. L. Solovjov[1], E. V. Petrenko[1], L. V. Omelchenko[1], R. V. Vovk[2], I. L. Goulatis[2] & A. Chroneos[3,4]

The effect of annealing both in the oxygen atmosphere and at room temperatures on physical properties such as the pseudogap ($\Delta^*(T)$) and excess conductivity ($\sigma'(T)$) of untwined $YBa_2Cu_3O_{7-\delta}$ (YBCO) single crystal with a small deviation from oxygen stoichiometry is studied. It was revealed that as the charge carrier density, n_f, increases, T_c also slightly increases, whereas the temperature of the pseudogap opening, T^*, decreases noticeably, which is consistent with the phase diagram (PD) of cuprates. The excess conductivity in the vicinity of T_c is represented by the Aslamazov-Larkin and Hikami-Larkin fluctuation theories, illustrating the three-dimensional to two-dimensional (i.e. 3D-2D) crossover with an increase in temperature. The crossover temperature T_0 determines the coherence length along the *c* axis is $\xi_c(0) = 0.86$ Å, that is 2.6 times larger than for optimally doped YBCO single crystals with defects. Taking into account the short coherence length in high-temperature superconductors, in the model of free charge carriers the phase relaxation time of fluctuating Cooper pairs is determined, $\tau_\varphi(100 K) = (4.55 \pm 0.4) \cdot 10^{-13}$ s, which is slightly (1.2 times) larger than in well-structured YBCO films, and as in films, does not depend on n_f. It is shown that $\Delta^*(T)$ at different annealing stages practically does not change its shape. As in the well-structured YBCO films, $\Delta^*(T)$ demonstrates maximum at $T_{pair} \sim 124$ K which depends weakly on n_f. However, the maximum value of $\Delta^*(T_{pair})$ increases with increasing n_f, as it follows from the PD of cuprates. Comparing the experimental data with the Peters-Bauer theory we estimated the density of local pairs $<n_\uparrow n_\downarrow> \approx 0.3$ near T_c that is a common value for high-temperature superconductors.

The mechanism of superconducting pairing in high-temperature superconductors (HTSCs), which makes it possible to obtain paired fermions at temperatures as higher as ~100 K, remains rather debatable[1–9]. To clarify the issue, the study of superconducting (SC) fluctuations has attracted considerable attention in the research of HTSCs[10–12] (and references therein). This because it is related to the nature of the pseudogap (PG), which is known to open in underdoped cuprates at a temperature T^*, much above the superconducting transition temperature T_c[2–5,8–11]. Above T^* the dc resistivity, $\rho(T)$, of optimally doped (OD) and moderately underdoped cuprates is known to be linear[13]. In the framework of the Nearly Antiferromagnetic Fermi Liquid model[14] it was proven that this linearity is a specific feature of HTSCs that is represented by the stability of the Fermi surface (FS). Notably, at $T < T^*$ not only all the properties of HTSCs measured by various experimental methods[15] change, but the density of electronic states at the Fermi level begins to decrease[16,17], which by definition is called a pseudogap[11,18]. It is also assumed that below the PG temperature T^* the rearrangement of the FS may begin[2,3,18,19]. Accordingly, at T^*, the resistivity curve deviates downward from the linearity leading to excess conductivity $\sigma'(T)$ as the difference between determined conductivity $\sigma(T) = 1/\rho(T)$ and extrapolated normal-state conductivity $\sigma_N(T) = 1/\rho_N(T)$[4,5,11,20,21].

Importantly, the SC fluctuations are responsible for a relatively short part of the entire excess conductivity, ~15 K above T_c, which is thus called the fluctuation conductivity (FLC)[10–12,20] (and references therein). In such a scenario, the long-range coherence is lost at T_c due to fluctuations of the phase of the superconducting order parameter[8,22,23]. The FLC region would then be marked by (preformed) fluctuating Cooper pairs (FCPs), which obey the Aslamasov-Larkin (AL)[24] and Hikami-Larkin (HL) (Maki-Thompson (MT) term)[25] fluctuation theories, and take the role of the precursor to the SC state[1,8,9]. In the FLC region, the FCPs behave in a good many way

[1]B. I. Verkin Institute for Low Temperature Physics and Engineering of National Academy of Science of Ukraine, 47 Nauki ave., 61103, Kharkov, Ukraine. [2]Physics Department, V. Karazin Kharkiv National University, Svobody Sq. 4, 61077, Kharkiv, Ukraine. [3]Department of Materials, Imperial College, London, SW7 2AZ, UK. [4]Faculty of Engineering, Environment and Computing, Coventry University, Priory Street, Coventry, CV1 5FB, United Kingdom. Correspondence and requests for materials should be addressed to A.C. (email: alexander.chroneos@imperial.ac.uk)

Sample	$\rho(100\,K)$ ($\mu\Omega cm$)	T_c (K)	$T_c^{\,mf}$ (K)	T_G (K)	T_o (K)	T_{01} (K)	ΔT_{fl} (K)	d_{01} (Å)	$\xi_c(0)$ (Å)	C_{3D}
A1	47.2	91.6	91.84	91.90	92.34	97.4	5.5	3.50	0.86	1.34
A2	47.0	91.7	91.93	91.98	92.39	96.9	4.9	3.54	0.84	1.25
A3	46.3	91.9	91.98	92.02	92.42	97.3	5.3	3.42	0.81	1.27

Table 1. Determined parameters.

like conventional SC pairs without the long-range coherence (known as "short-range phase correlations")[2,6,8,9], which have to obey the BCS theory[26]. The question is, what happens with the FCPs, which also called the local pairs (LPs)[11], with increasing temperature, as there are usually no any particularities on the resistive curve up to T*. In accordance with the theory of systems with reduced charge carrier density[27–30], along with an increase in T, the in-plane coherence length, $\xi_{ab}(T)$, which determines the pair size, decreases. At the same time, the bonding energy of the LPs, $\varepsilon_b \sim 1/\xi_{ab}^2$ [27,30], noticeably increases. As a result, the LPs should change their properties[9,11,29,30]. Eventually, the FCPs are transformed into so-called strongly bound bosons[9,28–30], very small but tightly coupled pairs, which obey the Bose-Einstein condensation theory[9,27,30]. Thus, the theory predicts the BCS-BEC transition in HTSCs as T increases, which was observed experimentally[11,12,31].

Nevertheless, there is still the question of the pairing mechanism, which allows the existence of bound fermions at temperatures significantly higher than T_c. Obviously, in HTSCs, in addition to the electron–phonon interaction, some other mechanism of interaction, most likely of a magnetic type should act[2–5,31] (and references therein). As a result, it is proposed to consider both spin-density waves (SDW)[2,3,18], charge-density waves (CDW)[2–5] and charge order (CO)[19] (and references therein) in order to explain the pairing mechanism of HTSCs in the PG state. However, in YBCO, the CO onset temperature appears always to be lower than T^{*} [19] and the temperature ranges and density of charge carriers indicated in the studies that assume the existence of the SDW, CDW and CO mechanisms differ significantly. As a result, the proposed new phase diagrams of cuprates are also very different[3–5,9,18,19]. Thus, despite the tremendous efforts towards this end there is still no consensus on the physical nature of the PG (refer to[1–11,18,19,28–32] and references therein).

It is well established now, that all properties of HTSC cuprates are determined by the density of charge carriers, n_f, which can vary over a wide range upon doping[2–5,10–13,18–21]. In $YBa_2Cu_3O_{7-\delta}$, n_f changes as a result of oxygen intercalation, and the maximum $T_c \sim 92\,K$ corresponds to a stoichiometric material (i.e. $\delta = 0$)[13]. To transfer YBCO to the so-called overdoped regime, it is necessary to use Ca doping[3]. Usually a set of samples with different n_f is used for measurements[10–13,20]. In the manufacture of HTSC films, each n_f value is determined by the manufacturing conditions (usually the oxygen pressure in the chamber) of each specific sample[19,33]. As a result, film samples may differ in their structure, number of defects etc. The advantage of single crystals is that their n_f can vary noticeably during annealing of the sample in an oxygen atmosphere[13,34]. However, in the case of a strong change in n_f, various defects may also appear in the samples[21,35] (cf. the thermodynamic parameters of defect processes in these high T_c superconductors have been found to obey the thermodynamical $cB\Omega$ model -where c stands for a dimensionless factor that may be considered in a first approximation to be independent of temperature and pressure, B is the isothermal bulk modulus and Ω the mean volume per atom[36,37] - in a similar fashion as in the case of the so-called superionic conductors e.g. β-PbF_2[38]). Therefore, it seems highly desirable to find out how the properties of the same sample, first of all FLC and PG, can change, if somehow the density of charge carriers in the sample varies in a relatively small range.

In the present study we take advantage of single crystals to study FLC and PG in untwined YBCO single crystal with n_f close to optimal doping ($T_c = 91.6\,K$), when n_f changes upon annealing in an oxygen atmosphere. We have studied three samples with different n_f. For a short notation, we name these samples A1, A2 and A3 (Table 1 and experimental methods). The fluctuation contributions to $\sigma'(T)$ were derived from the dc resistivity $\rho(T)$ measurements, and temperature dependences of PG, $\Delta^{*}(T)$, as a function of n_f were calculated. The results show that in the range of SC fluctuation near T_c, $\sigma'(T)$ is adequately interpreted by the AL and HL fluctuation theories. It was determined that $\Delta^{*}(T)$, as expected, increases upon annealing and is in good agreement with the Peters-Bauer theory (PB)[6] near (T_c). The implications of these findings will be discussed.

Results and Discussion

Resistivity. The dependence on temperature of the resistivity (i.e. $\rho(T) = \rho_{ab}(T)$) of untwined $YBa_2Cu_3O_{7-\delta}$ crystals are shown in Fig. 1. As $\rho(T)$ of the samples differ insignificantly, to simplify the figure on the upper panel (Fig. 1a), only the resistive curve of sample A1 is shown. The corresponding dependences of $\rho(T)$ for all three samples are shown as a three-dimensional (3D) graph in Fig. 1b. For temperatures above $T^{*} = (185 \pm 0.5)$ K (A1), (182 ± 0.5) K (A2), (179 ± 0.5) K (A3) and up to 300 K, all the $\rho(T)$ dependences are linear and are described by a gradient $a = d\rho/dT = 0.484$ (A1), 0.488 (A2) and 0.478 (A3) $\mu\Omega \cdot cm/K$, which slightly changes with annealing. The gradient was calculated by approximating the experimentally derived curves and confirmed the linear behaviour of $\rho(T)$ with a mean-root-square error of 0.009 ± 0.002 in the specified temperature range for all samples. As mentioned above, the PG temperature $T^{*} \gg T_c$ was defined as a temperature at which the resistive curve deviates downward from the linearity (Fig. 1). The more precise approach to determine T^{*} with accuracy ± 1 K is to explore the criterion $[\rho(T) - \rho_0]/aT = 1$ [39] (insert in Fig. 1a), where a designates the slope of the extrapolated normal-state resistivity, $\rho_N(T)$, and ρ_0 is its intercept with the y axis. Both methods give the same T^{*}.

In the process of annealing, with increasing the oxygen content, T_c slightly increases, and $\rho(T)$ slightly decreases (Fig. 1b). This is not surprising, since the samples are actually on top of the PD. At the same time, T^{*} decreases much more perceptibly, in full agreement with the PD of cuprates[3–5,13,18,21] (and Tables 1, 2 and 3). The main difference between the untwined YBCO and single crystal containing defects, presumably in the form of
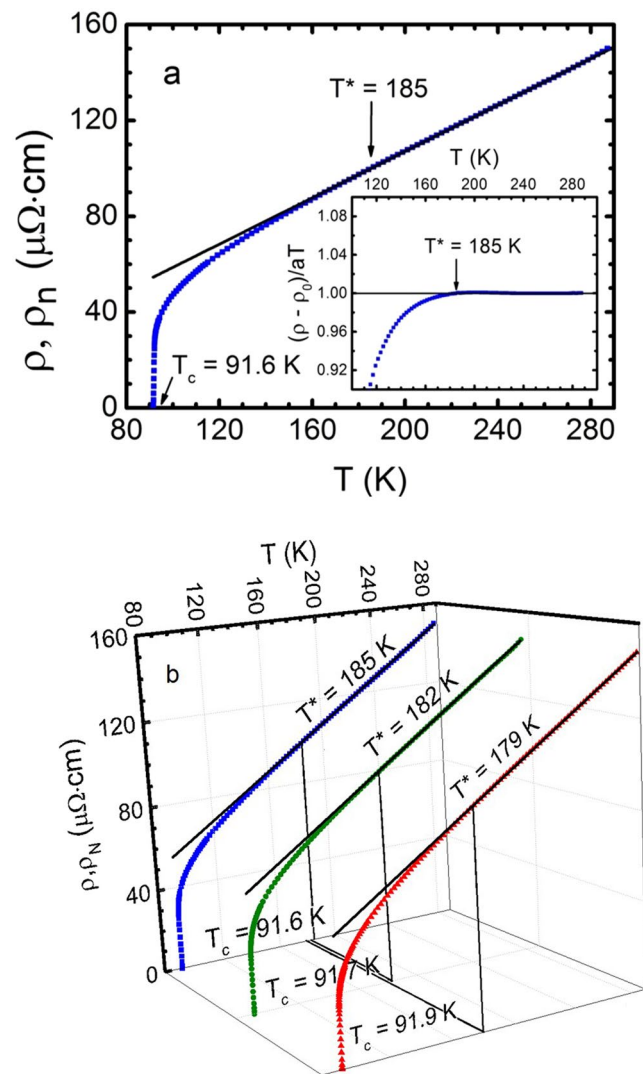
Figure 1. Panel a. Plot of $\rho(T)$ dependence for untwined $YBa_2Cu_3O_{7-\delta}$ single crystal after annealing in oxygen (sample A1, squares). Insert: The method of determining T*, using criterion $[\rho(T) - \rho_0]/aT = 1$ (sample A1)[39]. Panel b. The plot of $\rho(T)$ of the same single crystal for different annealing stages: A1 (blue squares), A2 (green dots) and A3 (red triangles). The solid lines determine $\rho_N(T)$, extrapolated to the low-temperature region.

Sample	$R_H(100\,K)$ $(10^{-9}m^3/C)$	$\rho(100\,K) \cdot C_{3D}$ $(\mu\Omega cm)$	n_f $(10^{21}\,cm^{-3})$	n_s $(10^{14}\,cm^{-2})$	μ_H (cm^2/Vs)	l $(10^{-8}\,cm)$
A1	2.40	62.9	2.60	3.05	38.2	110.0
A2	2.39	58.6	2.62	3.06	40.8	117.8
A3	2.38	58.8	2.63	3.07	40.5	117.1

Table 2. Determined parameters.

twin boundaries (TB)[21,40], is much higher T* value. Usually, in optimally doped YBCO single crystals with $T_c \sim$ 91.1 K, but containing defects in the form of TB, T* $\sim$ 140 K[41]. It is assumed that the defects prevent the establishment of phase coherence of LPs (paired fermions) and, thus, effectively reduce T*[21,42]. At the same time, in well-structured YBCO films[11,20], a sample with $T_c \sim$ 88 K has T* $\sim$ 200 K, which is much closer to T* = 185 K, observed for the untwined YBCO single crystal A1 with $T_c = 91.6$ K. Therefore, it can be assumed that, by their properties, YBCO single crystals, which do not contain TB, are closer to well-structured films. This conclusion is supported by the analysis of the results of the FLC and PG study.

Fluctuation conductivity. In the resistive measurements, PG is evident as a deviation of the resistivity $\rho_{ab}(T) = \rho(T)$, determined in the *ab* plane, from a linear dependence at high temperatures to smaller values (refer to Fig. 1). The result is excess conductivity expressed by $\sigma'(T) = \sigma(T) - \sigma_N(T) = [1/\rho(T)] - [1/\rho_N(T)]$, or

Sample	ξ_{ab} (Å)	v_F (10^7 cm/s)	m^*/m_0	τ (100 K) (10^{-13} s)	τ_φ (100 K) β (10^{-13} sK)	β	τ_φ (100 K) (10^{-13} s)
A1	11.00	1.04	4.91	1.06	54.68	12.03	4.55
A2	10.50	1.01	5.04	1.17	59.83	13.49	4.43
A3	10.35	1.04	4.92	1.13	60.73	13.61	4.46

Table 3. Determined parameters.

$$\sigma'(T) = [\rho_N(T) - \rho(T)]/[\rho(T)\rho_N(T)], \tag{1}$$

where $\rho_N(T) = aT + b$ is the sample resistivity in the normal state that is extrapolated to the low temperature region[4,5,20,43]. As mentioned above, according to the model[14], the linear dependence of $\rho(T)$ above T* is the normal state of HTSCs that characterizes by the stability of the FS[2,3,14,19].

According to recent concepts[4–11,21], a small value of the coherence length in conjunction with a quasi-layered structure of the HTSCs leads to the formation of a noticeable area of SC fluctuations on the $\rho(T)$ in the proximity of T_c, where $\sigma'(T)$ follows conventional fluctuation theories[11,20,44–46]. At the same time, changes in oxygen content, the presence of impurities, and/or structural defects have a considerable impact on $\sigma'(T)$ and, accordingly, on the implementation of various FLC modes above T_c[20,47–49].

Fluctuation conductivity for (or of) all the samples was determined by analyzing the excess conductivity, which was calculated in the standard method in accordance with Eq. (1). The FLC analysis was performed within the model of local pairs[1,11,20,21], in which the presence of paired fermions (LPs) in HTSCs is assumed in the temperature range $T_c < T < T*$[1,6–9,20]. Firstly, the mean-field temperature $T_c^{mf} > T_c$ needs to be determined limiting the region of critical fluctuations near T_c, where the mean-field theory does not work[26]. In addition, T_c^{mf} determines the reduced temperature

$$\varepsilon = \frac{T - T_c^{mf}}{T_c^{mf}} \tag{2}$$

that appears in all equations. From this it is clear that the correct determination of T_c^{mf} plays a key role in the calculations of both FLC and PG. At the vicinity of T_c, the coherence length in the c axis ($\xi_c(T)$) is greater than d. d ≈ 11.7 Å[50] is the c axis lattice parameter of the YBCO unit cell[25,46]. In this case, the FCPs associate throughout the superconductor and form a three-dimensional (3D) state of HTSC[20,25,46]. Therefore, at the proximity of T_c, the FLC can be described by the 3D equation of the Aslamazov-Larkin (AL) theory[11,24] with the critical exponent $\lambda = -1/2$, which determines the FLC in any 3D system:

$$\sigma'_{AL3D} = C_{3D} \frac{e^2}{32\hbar\xi_c(0)} \varepsilon^{-\frac{1}{2}} \tag{3}$$

Here $\sigma'(T) \sim \varepsilon^{-1/2}$. It can be shown that $\sigma'^{-2}(T) \sim \varepsilon \sim T - T_c^{mf}$ and vanishes at $T = T_c^{mf}$ (refer to Fig. 2), which enables the determination of both T_c^{mf} and ε with high accuracy[11,20,51]. Also in Fig. 2, the arrows show T_c, the Ginzburg temperature T_G, down to which the fluctuation theories are valid[46,47], and the T of the 3D-2D crossover T_0 limiting the area of 3D fluctuations. Notably, above $T_0 = 92.34$ K (refer to Fig. 2), the data deviate to the right from the linear dependence, which indicates the presence of 2D Maki-Thompson (MT) contribution to the FLC[25,46]. Having determined ε, we construct the dependence $\ln\sigma'(\ln\varepsilon)$ (Fig. 3). Figure 3a shows the corresponding dependence for the base sample A1. Expectedly at the vicinity of T_c, in the interval T_G — T_0 ($\ln(\varepsilon_0) = -5.21$), the FLC is well modelled by the AL fluctuation contribution (3) for the 3D system. In double logarithmic coordinates this is the dashed line (1) with slope $\lambda = -1/2$. As mentioned above, it implies that the classical three-dimensional FLC materializes in HTSC for $T \to T_c$ and $\xi_c(T) > d$[11,20,43]. Above the crossover temperature $T_0 \xi_c(T) < d$[11,21,25,46], and this is no longer a 3D regime. However, as before, $\xi_c(T) > d_{01}$, where $d_{01} \approx 3.5$ Å is the separation of the conducting planes of CuO$_2$ in YBCO[50]. Thus, up to temperature T_{01} ($\ln(\varepsilon_{01}) = -2.8$, Fig. 3) $\xi_c(T)$ connects the inner planes of CuO$_2$ by means of the Josephson interaction[11,20,46]. This is the 2D FLC regime, which is perfectly approximated by the Hikami-Larkin theory 2D-MT equation for HTSCs[25]:

$$\sigma'_{MT2D} = \frac{e^2}{8d\hbar}\frac{1}{1 - \alpha/\delta}\text{ln}\left[(\delta/\alpha)\frac{1 + \alpha + \sqrt{1 + 2\alpha}}{1 + \delta + \sqrt{1 + 2\delta}}\right]\varepsilon^{-1} \tag{4}$$

Above T_{01}, the experimental points deviate downward from the theory (Fig. 3) implying that the classical fluctuation theories are not valid. Thus, T_{01} limits the region of SC fluctuations from above: $\Delta T_{fl} = T_{01} - T_G$. Conversely, T_G limits the region of SC fluctuations from below. As a result, below T_G, designated as $\ln(\varepsilon_G)$ in (Fig. 3a,b), the experimental points also deviate downward from the theory (Fig. 3), suggesting the transition to the range of critical fluctuations or fluctuations of the SC order parameter Δ just near T_c, where $\Delta < kT$[11,26].

The thin curves (3) in the figure are constructed according to the Lawrence-Doniach equation (LD)[44]:

$$\sigma'_{LD} = C_{LD}\frac{e^2}{16\hbar d\sqrt{1 + 2\alpha}}\varepsilon^{-1} \tag{5}$$
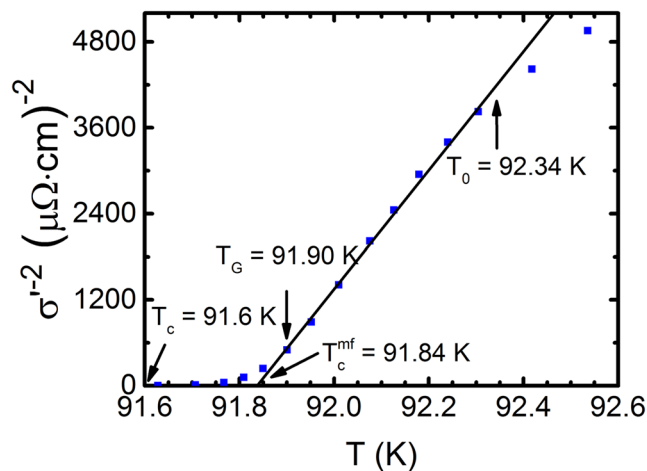
Figure 2. Dependence of $\sigma'^{-2}(T)$ for the untwined $YBa_2Cu_3O_{7-\delta}$ single crystal after annealing in oxygen (sample A1). Arrows indicate T_c, T_c^{mf}, the Ginzburg temperature T_G and 3D-2D crossover temperature T_0. A straight line is to guide the eye.
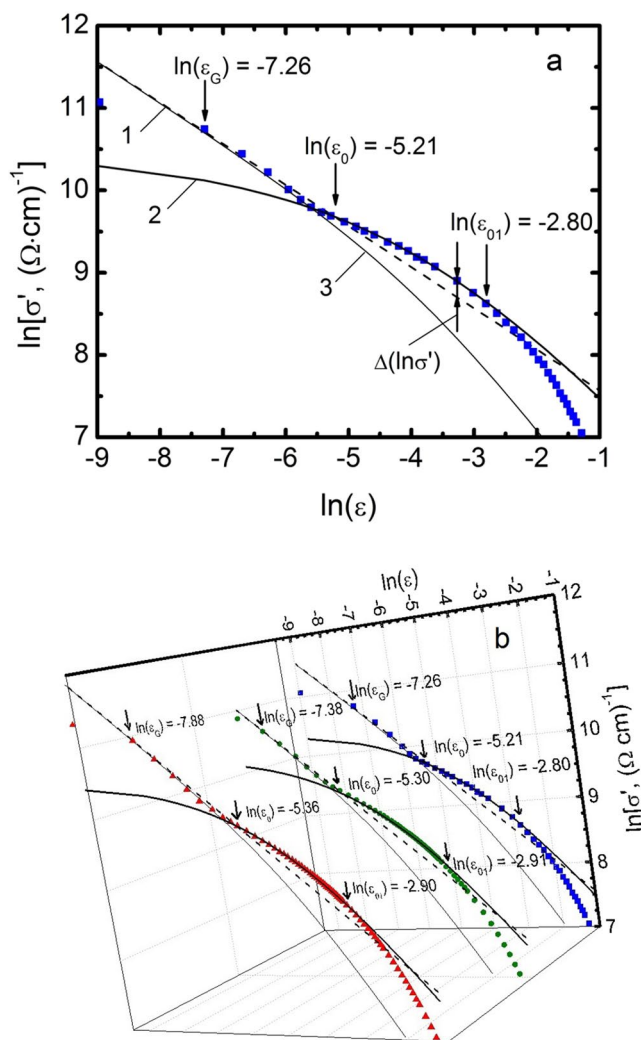
Figure 3. Panel a. $\ln\sigma'$ vs $\ln\varepsilon$ for the sample A1 (squares) in comparison with fluctuation theories: 3D AL (dashed line (1)), 2D MT (solid curve (2)) and LD (solid thin curve (3)). The T_{01} ($\ln\varepsilon_{01}$) determines the range of the SC fluctuations, T_0 ($\ln\varepsilon_0$) is the temperature of the 3D-2D crossover and T_G ($\ln\varepsilon_G$) is the Ginzburg temperature. Panel b: The same dependencies for all three samples: A1 - blue squares, A2 - green dots and A3 - red triangles.

The LD model works in case of defects in samples[21,42,51]. In our case, curves (3) lie far from the experimental points, which confirm the absence of defects (primarily TB) in our samples.

Notably, in this case the maximum distance between the MT curve (2) and the extrapolated AL straight line (1), $\Delta \ln \sigma' \sim 0.1$, which is typical for nonmagnetic YBCO[11,20]. In magnetic superconductors, such as $SmFeAsO_{0.85}$, the MT curve (2) always passes much higher than the extrapolated AL straight line (1)[11], and in this case $\Delta \ln \sigma' \sim 0.8$[31]. Such behavior indicates the presence of a magnetic interaction in HTSCs, which is clearly absent in our non-magnetic untwined single crystal.

At T_0, $\xi_c(T_0) = d = 11.7$ Å, which allows us to determine $\xi_c(0)$[20,21,25,46]

$$\xi_c(0) = d\sqrt{\varepsilon_0} \qquad (6)$$

Taking into account that $\ln(\varepsilon_0) = -5.21$ (Fig. 3) and using Eq. (6), we get $\xi_c(0) = (0.86 \pm 0.02)$ Å (A1), which is almost 2.6 times the coherence length alongside the c axis obtained for OD YBCO with TB ($T_c = 91.07$ K)[41]. This is most likely due to the fact that in single crystals with defects the region of SC fluctuations is $\Delta T_{fl} = T_{01} - T_G \sim 1.5$ K, that is extremely small. While for A1, $\Delta T_{fl} = T_{01} - T_G = 97.4$ K $- 91.9$ K $= 5.5$ K, that is, 3.7 times more. The result again underlines a noticeable difference in the behavior of YBCO single crystals with and without defects. Additionally, $\xi_c(T_{01}) = d_{01}$, and, since $\xi_c(0)$ has already been defined by Eq. (6), we can calculate d_{01} from the relation $\xi_c(0) = d\sqrt{\varepsilon_0} = d_{01}\sqrt{\varepsilon_{01}}$. For sample A1, calculations give $d_{01} = (3.5 \pm 0.2)$ Å, in good agreement with the results of structural studies[50].

In Fig. 3b the dependences of $\ln\sigma'(\ln\varepsilon)$ are shown for all three samples A1–A3. It is seen that with increasing T_c all characteristic temperatures also vary slightly. The increase in the absolute value of $\ln\varepsilon_0$ results in decrease in $\xi_c(0)$ from 0.86 Å (A1) to 0.81 Å (A3) (Table 1), in full agreement with the theory of superconductivity, where $\xi \sim 1/T_c$[26].

In the above equations

$$\alpha = 2\left(\frac{\xi_c(0)}{d}\right)^2 \varepsilon^{-1} \qquad (7)$$

is the coupling parameter;

$$\delta = \beta \frac{16}{\pi\hbar}\left(\frac{\xi_c(0)}{d}\right)^2 k_B T \tau_\varphi \varepsilon^{-1} \qquad (8)$$

is the pair-breaking parameter, and the phase relaxation time τ_φ is determined by the equation

$$\tau_\varphi \beta T = \pi\hbar/8k_B\varepsilon = A/\varepsilon \qquad (9)$$

where $A = 2.998 \cdot 10^{-12}$ s K. Here the factor $\beta = 1.203(l/\xi_{ab})$ with l being the mean free path and ξ_{ab} the coherence length along the *ab* plane, takes into account the approximation of the clean limit ($l > \xi$) that consistently occurs in HTSCs due to the smallness of $\xi(T)$[25,44–46].

Comparative analysis of phase relaxation time. Having determined the parameters of the FLC analysis, it seems interesting to examine the physical meaning of the short coherence length $\xi_{ab}(0)$ in the framework of the simple two-dimensional model of free charge carriers[52–54]. This approach allows us to define a set of additional important parameters of the samples, including τ_φ, which is actually the lifetime of the FCPs in the range of SC fluctuation. In HTSCs all parameters, including τ_φ and Hall coefficient R_H, are functions of temperature. Consequently, the corresponding calculations, including those in YBCO, are performed at T = 100 K, as is customary in the literature[20,52–54].

From the FLC analysis, using Eq. (7), we find the coupling parameter α, and then the pair-breaking parameter δ of Eq. (8), which is always ~ 2[20,54], if all other parameters are correctly determined. Next, we calculate the parameter $\tau_\varphi \beta T$ (refer to Table 3), assuming in Eq. (9) $\varepsilon = \varepsilon_0$[20]. Since it is assumed that T = 100 K, in order to find $\tau_\varphi(100$ K), it is necessary to determine the coefficient $\beta = 1.203(l/\xi_{ab})$. For this it is necessary to know the mean free path l, which is determined by the density of charge carriers n_f, and the coherence length in the *ab* plane (i.e. ξ_{ab}). The charge carrier density n_f can be calculated from the values of the Hall coefficient R_H, namely $n_f = r [l/(e R_H)]$[20,54,55]. Here e is the electron charge, and the coefficient $r = <\tau^2>/<\tau>^2$, where τ is the average time between collisions of charge carriers, actually determines the scattering mechanism in the normal state[55]. Since the scattering mechanism of normal charge carriers in HTSCs, especially in the PG state, is still rather uncertain[56–59], we assume $r = 1$.

From the literature for optimally doped YBCO single crystals[3,60] and YBCO films with a close value of T_c[20], we find: $R_H(100$ K$) \approx 2.4 \cdot 10^{-9}$ m³/C for sample A1, and, accordingly, $n_f = 2.6 \cdot 10^{21}$ см⁻³ (Table 2). Continuing the analysis of sample A1, for the carrier density in the planes we obtain $n_s = n_f d = 3.05 \cdot 10^{14}$ см⁻³. Using the corrected value $\rho(100$ K$) = \rho(100$ K$) \cdot C_{3D} = 62.9$ μΩcm[52,53], we have $\mu_H = r/(\rho ne) = 38.2$ cm²/Vs for the mobility of the Hall carriers. Interestingly, found values of μ_H (Table 2) are in good agreement with those obtained in ref.[60] for YBaCuO untwinned single crystals. It was also shown[60] that the results of Hall-effect measurements are nor affected by the conduction of the Cu-O chains and the in-plane anisotropy of the CuO_2 planes. Now, using the formula $l = (\hbar\mu/e)(2\pi n_s)^{1/2}$, we find the mean free path of the charge carriers in A1: $l = \upsilon_F \tau \approx 110$ Å, where υ_F is the Fermi velocity. To continue the analysis, the mean value $\xi_{ab}(0) = 11.0$ Å was chosen for A1 from the literature[51–53].

In the general theory of superconductivity[26]

$$\xi_0 \sim \hbar\upsilon_F/[\pi\Delta(0)] \tag{10}$$

where $\Delta(0)$ is the SC order parameter at $T = 0$ K. Taking into account that in YBCO $\Delta(0)/k_B T_c = 5$[54,61,62] and setting $\xi_0 = \xi_{ab}(0)$, for the Fermi velocity we obtain $\upsilon_F = 1.04\cdot10^7$ cm/s, and for the effective mass of charge carriers $m^*/m_0 = (\rho l)(n_f e^2)/(\upsilon_F m_0) = 4.91$ (Table 3). After this, the transport time of the normal carriers $\tau(100\,K) = l/\upsilon_F = 1.06\cdot10^{-13}$ s can also be calculated. All estimates obtained are in good agreement with the similar results reported for optimally doped YBCO[20,52-54,58,59].

Finally, we find $\beta\,(100\,K) = [1.203(l/\xi_{ab})] = 12.03$. Now, using found $\tau_\varphi\,(100\,K)\beta = 54.68\cdot10^{-13}$ sK, we get the value of $\tau_\varphi\,(100\,K) = 4.55\cdot10^{-13}$ s. Performing similar calculations for samples A2 and A3 and taking into account the corresponding changes of R_H and $\xi_{ab}(0)$ with increasing n_f (Tables 2 and 3), we obtain $\tau_\varphi\,(100\,K) = 4.43\cdot10^{-13}$ s and $\tau_\varphi\,(100\,K) = 4.46\cdot10^{-13}$ s (Table 3) in good agreement with similar results obtained by measuring the magnetoresistance on YBCO-PrBCO superlattices[63] and FLC on YBCO films[20].

Nevertheless, the mean free path l and the Hall mobility μ_H are about 2 times, and $\tau_\varphi(100\,K)$ is ~ 1.2 times more than in OD YBCO films[20], which is most likely a specific property of untwined single crystals[60]. At the same time $\tau_\varphi\,(100\,K)/\tau\,(100\,K) \sim 4 \pm 0.2$, in excellent agreement with the theory[45], which takes into account the clean-limit approximation ($l > \xi$), as mentioned above. It should be emphasized that, as in well-structured YBCO films with different n_f[20], in the untwined single crystals $\tau_\varphi(100\,K)$ is practically independent on n_f. This result, apparently, can be considered as a common property of cuprates, at least of compounds based on YBCO.

Pseudogap analysis. In resistive measurements of cuprates the pseudogap is a deviation at $T \leq T^*$ of the longitudinal resistivity $\rho(T)$ from linearity in the normal phase[11,14,64]. This results to the realization of excess conductivity $\sigma'(T)$ (refer to Eq. (1)). It is established that if there were no processes in HTSC leading to the opening of the PG at T^*, then $\rho(T)$ would preserve its linearity up to $T \sim T_c$[4,11,14,27-30]. It is obvious that $\sigma'(T)$ is a consequence of the PG opening and should enclose details about the magnitude and temperature dependence of the PG[11,23]. Conventional fluctuation theories, modified by Hikami-Larkin[25] for HTSCs perfectly describe the experimental $\sigma'(T)$ but only to about ~110 K[10,11,31]. For complete information about the pseudogap, an equation is needed that would describe the experimental curve in all temperature range from T^* to T_c and would contain PG explicitly. Such an equation was proposed earlier[12]:

$$\sigma'(\varepsilon) = \frac{e^2 A_4\left[1 - \frac{T}{T^*}\right]\left[exp\left(-\frac{\Delta^*}{T}\right)\right]}{16\hbar\xi_c(0)\sqrt{2\varepsilon_{c0}^*}\ \sinh(2\varepsilon/\varepsilon_{c0}^*)} \tag{11}$$

where $(1 - T/T^*)$ takes into consideration the number of LPs formed at $T \leq T^*$, and $(exp(-\Delta^*/T))$ determines the dynamics of LPs destruction as T approaches T_c.

Additionally to T^*, ε and $\xi_c(0)$, already defined above, Eq. 11 includes the numerical coefficient A_4, which is equivalent to the C-factor in the FLC theory[20,51-53], the theoretical parameter $\varepsilon_{c0}*$[65] and $\Delta^* = \Delta^*(T_G)$. Here it is presumed that $\Delta^*(T_G) = \Delta(0)$[66,67] with Δ being the order parameter of the sample in the SC state, as mentioned above. Importantly, all these parameters can be easily determined within the LP model[11,12,20,31]. We consider this for the case of A1 (refer to Figs 4, 5). In the region $\ln\varepsilon_{c01} < \ln\varepsilon < \ln\varepsilon_{c02}$ or, respectively, $\varepsilon_{c01} < \varepsilon < \varepsilon_{c02}$ (113 K < T < 155 K), $\sigma'^{-1} \sim \exp(\varepsilon)$[65]. This feature turned out to be one of the main properties of most HTSCs[11,31,54]. As a result, in the specified temperature range, $\ln\,(\sigma'^{-1})$ depends linearly with respect to ε with a slope $\alpha^* = 5.8$ (insert to Fig. 4a), which determines the parameter $\varepsilon_{c0}* = 1/\alpha^* = 0.172$[65]. This allows the determination of reliable values of $\varepsilon_{c0}*$ for all samples, which, as established previously[12,31], significantly impacts the dependence of the theoretical curves shown in Figs 4 and 5, at high T.

To determine A_4, we approximate the experiment by the dependence $\sigma'(\varepsilon)$ calculated by Eq. (11), in the vicinity of 3D AL-fluctuations near T_c (refer to Fig. 4). $\ln\sigma'(\ln\varepsilon)$ is in essence a linear dependence of ε (i.e. the reduced temperature) and has a slope $\lambda = -1/2$. To find $\Delta^*(T_G)$ used in Eq. (11), we construct the curve $\ln\sigma'(1/T)$ using all the parameters found[68] (refer to Fig. 5). Here, the gradient of the theoretical curve (11) is highly influenced by the value of $\Delta^*(T_G)$[12,20,31]. The best approximation is achieved when the Bardeen-Cooper-Schrieffer (BCS) ratio $D^* = 2\Delta^*(T_G)/k_B T_c$ is 5.0 ± 0.1, which corresponds to the strong-coupling limit characteristic for YBCO. Accordingly, we obtain: $\Delta^*(T_G)/k_B \approx 229$ K in good agreement with the experimental value $\Delta^*(T_G)/k_B \approx 228$ K (see Fig. 6). Similar results were obtained for samples A2 and A3 (refer to Table 4).

Solving equation (11) for the PG, $\Delta^*(T)$, we obtain[11,12] over the entire temperature range from T^* to T_c^{mf}

$$\Delta^*(T) = T\ \text{In}\frac{e^2 A_4\left(1 - \frac{T}{T^*}\right)}{\sigma'(T)16\hbar\xi_c(0)\sqrt{2\varepsilon_{c0}^*}\ \sinh(2\varepsilon/\varepsilon_{c0}^*)} \tag{12}$$

Here $\sigma'(T)$ is the experimentally determined excess conductivity and the remaining parameters are already defined within the LP model (Tables 1 and 4). The fact that $\sigma'(T)$ is given by Eq. (11) (refer to Fig. 4) suggests that Eq. (12) gives reliable values of both the magnitude and the temperature dependence of $\Delta^*(T)$. The dependence $\Delta^*(T)$ for sample A1, constructed by the formula (12), using the following parameters extracted from the experiment: $T_c^{mf} = 91.84$ K, $T^* = 185$ K, $\xi_c(0) = 0.86$ Å, $\varepsilon_{c0}* = 0.17$, $A_4 = 33$, $\Delta^*(T_G)/k_B = 229$ K, shown in Fig. 6. Also shown are the dependencies $\Delta^*(T)$ for samples A2 and A3, calculated in a similar way with the corresponding set of parameters given in Tables 1 and 4.

All the curves in Fig. 6 have the shape typical for YBCO films, with a maximum at $T = T_{pair} \approx 124$ K, which is close to $T_{pair} \approx 130$ K usually observed in well-structured YBCO films[12,54], and a minimum at $T \approx T_{01}$[31,41]. It can be
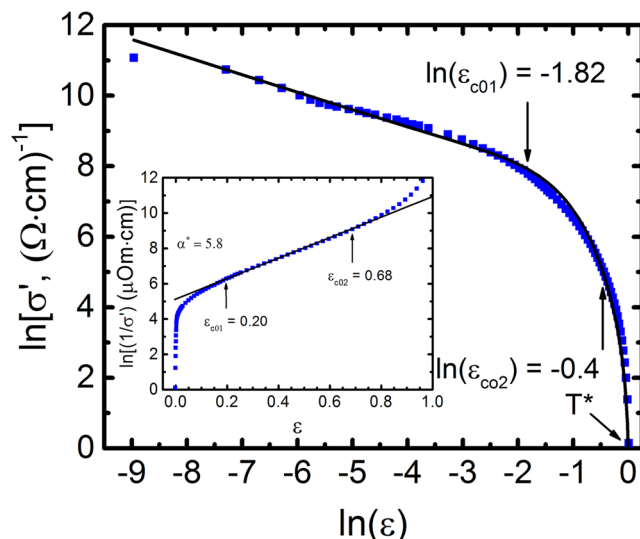
Figure 4. $\ln\sigma'$ vs $\ln\varepsilon$ (squares) for the untwined $YBa_2Cu_3O_{7-\delta}$ single crystal (sample A1) in the whole temperature range from T^* to T_G. The solid curve is fit to the data with equation (11) with the set of parameters given in the text. $\ln(\varepsilon_{c01})$ and $\ln(\varepsilon_{c02})$ designate the interval of exponential dependence of $\sigma^{-1}(\varepsilon)$. In the inset: $\ln(1/\sigma')$ with respect to ε[65]. Solid line indicates the linear part of the curve between $\varepsilon_{c01} = 0.20$ and $\varepsilon_{c02} = 0.68$. Corresponding $\ln(\varepsilon_{c01}) = -1.82$ and $\ln(\varepsilon_{c02}) = -0.4$ are marked by arrows in the main panel. $\alpha^* = 5.8$ is used to determine the parameter $\varepsilon^*_{c0} = 1/\alpha^* = 0.17$.
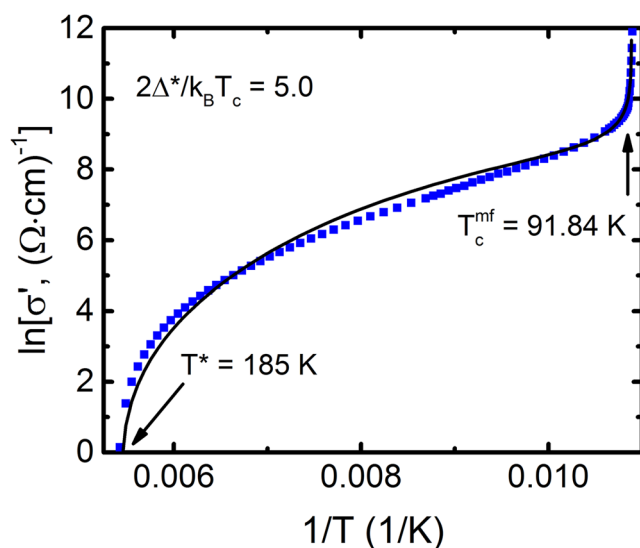

Figure 5. $\ln\sigma'$ as a function of $1/T$ (squares) for the sample A1 in the interval from T^* to T_c^{mf}. The solid curve is fit to the data with equation (11) with a set of parameters given in Tables 2, 3 and 4. The best fit is obtained when Eq. (11) is calculated with $\Delta^*(T_G) = 229$ K, that is $D^* = 2\Delta^*(T_G)/k_BT_c = 5.0$.

Sample	T^* (K)	α^*	ε^*_{c0}	A_4	$\Delta^*(T_G)$ (K)	$\Delta^*_{max}(T_{pair})$ (K)	T_{pair} (K)	D^* (K)
A1	185	5.8	0.17	33	229	258	119.3	5.0
A2	182	5.9	0.17	33	237	264	120.6	5.1
A3	179	5.8	0.17	37	244	270	120.7	5.3

Table 4. Experimental Parameters.

seen that, in full accordance with the phase diagram of cuprates, $\Delta^*_{max}(T_{pair})/k_B$ expectedly increases from 258 K (A1) to 270 K (A3) along with an increase in n_f. The BCS ratio $D^* = 2\Delta^*(T_G)/k_BT_c$ also increases from 5.0 to 5.3. At the same time, T_{pair} practically does not change (Table 4), which is reasonable, given the high T_c of the samples.
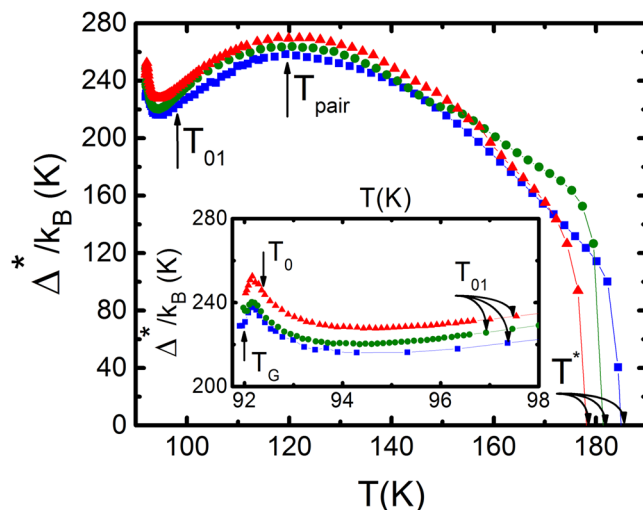
Figure 6. Temperature dependences of $\Delta^*(T)$, of the untwined $YBa_2Cu_3O_{7-\delta}$, single crystal, calculated by Eq. (12) for all annealing stages: A1 - blue squares, A2 - green points, A3 - red triangles. Inset: The same dependence for the temperature interval $T_G < T < T_{01}$. The arrows show all characteristic temperatures. Solid lines are to guide the eye.

As mentioned above, according to the theory of systems with low n_f[8,9,27–30], above T_{pair}, LPs must exist in the form of strongly bound bosons, which obey BEC. Below T_{pair} the LPs must be converted to FCPs, which are subject to BCS theory. Thus, T_{pair} separates both regimes[8–12,28–30]. The minimum $\Delta^*(T)$ at $T \approx T_{01}$ is also observed on all HTSCs, including pnictides[11] and single crystals of FeSe[69]. Accordingly, when approaching to T_c, the maximum $\Delta^*(T)$ always occurs just below T_0, and the minimum at $T = T_G$[31,41] (inset in Fig. 6). Below T_G, there is an abrupt jump $\Delta^*(T)$ at $T \rightarrow T_c^{mf}$, however, this is already a transition to the region of critical fluctuations, where the LP model does not work. Thus, the approach in the framework of the LP model makes it possible to determine the exact values of T_G and, as a consequence, to obtain reliable values of $\Delta^*(T_G) \approx \Delta^*(T_c) \approx \Delta(0)$[12,54,65–67] (Table 4).

It is noteworthy that the shape of the $\Delta^*(T)$ curves near T_c, shown in the inset to Fig. 6, is very similar to the temperature dependence of the density of local pairs in HTSCs, $<n_\uparrow n_\downarrow>$, calculated within the three-dimensional attractive Hubbard model for different temperatures, interactions $U > 0$, and filling factors (the Peters-Bauer model (PB)[6]). Besides, in the calculations the hopping t and the bandwidth $W = 12t$ were used as energy scales. Taking into account the fact that Eq. (12) contains information on the density of local pairs, we tried to compare our data with the results of the PB theory ref.[6]. Having normalized the temperature and PG, respectively, by $T^*(T)$ and Δ^*_{max}, and having adjusted the parameters, we obtained good agreement with the PB theory (refer to Fig. 7). In the process of fitting, $\Delta^*(T_G)/\Delta^*_{max}$ was coincided with the minimum value $<n_\uparrow n_\downarrow>$ at the lowest T, and $\Delta^*(T_0)/\Delta^*_{max}$ with the maximum value. Both temperatures in Fig. 7 are indicated by arrows. On the theoretical curve 2, these temperatures are indicated by inclined arrows. Importantly, the same fitting factors were used for all samples.

After fitting, good agreement was found between the experimental $\Delta^*(T)/\Delta^*_{max}$ and the theory of PB with the lowest interaction parameter $U/W = 0.2$, which corresponds to the density of local pairs $<n_\uparrow n_\downarrow> \approx 0.3$ near T_c (Fig. 7). As in the PB theory, the density of LPs in our samples increases (from $<n_\uparrow n_\downarrow> (T_G) \approx 0.292$ (A1) to $<n_\uparrow n_\downarrow> (T_G) \approx 0.305$ (A3)) with an increase in the interaction energy, which corresponds to an increase in the BCS ratio D^* in our case. As the temperature increases both $<n_\uparrow n_\downarrow>$ and our data, as expected, decrease (refer to Fig. 7), which seems reasonable. Indeed, the number of FCPs should decrease along with T[3–6,11]. Importantly, at $U/W = 0.2$ the experimental data is consistent with theory in a wide temperature range, actually in the whole range of SC fluctuations. Whereas, if we compare the data with the theory for larger values of U/W (curves 2 and 3), the data will deviate from the theory already at $T/W \sim 0.2$. Notably, $<n_\uparrow n_\downarrow> \approx 0.3$ was also obtained for FeSe single crystals near T_c[69]. Apparently, such a density of LPs near T_c is typical of all HTSCs.

Conclusions. Using the LP model, we have studied the effect of annealing on the temperature dependences of FLC and PG in untwined OD $YBa_2Cu_3O_{7-\delta}$ (YBCO) single crystal with a slight increase in the oxygen index (7-δ). The increase in oxygen content and, respectively, n_f was carried out by annealing the single crystal both in an oxygen atmosphere (sample A1) and by exposure at room temperature (samples A2 and A3). It is found that with increasing n_f in the sample, T_c increases, and resistivity decreases. As expected, the increase in T_c is rather small, since n_f actually corresponds to the maximum of the phase diagram (PD). At the same time, T^* decreases more significantly (from 185 K to 179 K), which fully corresponds to PD of the cuprates. The first difference from optimally doped YBCO single crystals containing defects in the form of TB, where $T^* \sim 140$ K[41], is quite large $T^* = 185$ K (A1). It is assumed that defects interfere with the establishment of phase coherence of LPs (paired fermions) and, thus, effectively reduce T^*[21,42]. Importantly, in well-structured YBCO films, the sample with $T_c \sim 88$ K has $T^* \sim 200$ K, which is much closer to $T^* = 185$ K, observed for A1. This result suggests the conclusion that the investigated properties of untwined YBCO single crystals are noticeably closer to the well-structured films, which was confirmed by the results of analysis of both FLC and PG.
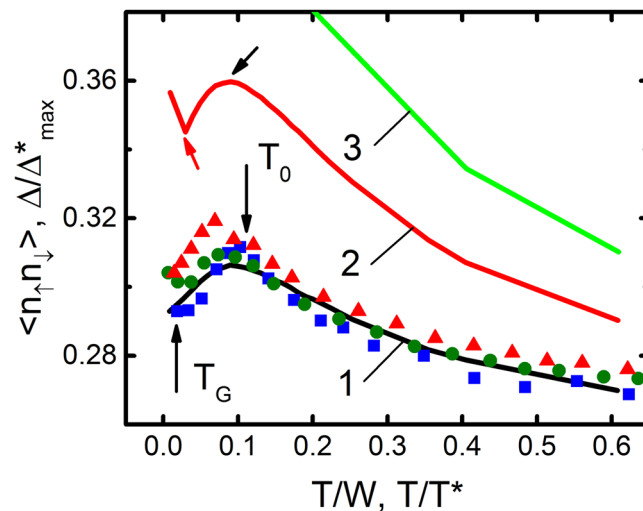
Figure 7. Solid curves display the density of local pairs $<n_\uparrow n_\downarrow>$ as a function of temperature for different values of the interaction energy: $U/W = 0.2$ (curve 1), $U/W = 0.4$ (curve 2) and $U/W = 0.6$ (curve 3)[6]. The symbols are experimental data for A1 (blue squares), A2 (green points), and A3 (red triangles), after corresponding renormalizations of the dependence $\Delta^*(T)$ in the interval $T_G < T < T_{01}$ (see Text).

The present study demonstrated that in the range of SC fluctuations near T_c FLC is consistent with the fluctuation theories of Aslamazov-Larkin (3D term) and Hikami-Larkin (2D-MT term), and demonstrate a 3D-2D crossover when the temperature is increased. T_0 determines $\xi_c(0) = 0.86$ Å (A1), which is 2.6 times higher than in optimally doped defective YBCO single crystals. This is most likely due to the fact that the range of FLC is very small: $\Delta T_{fl} = T_{01} - T_G = 97.4$ K $- 91.9$ K $= 5.5$ K (A1), which, however, is 3.7 times more than in single crystals containing defects, where $\Delta T_{fl} \sim 1.5$ K[41]. According to the theory[8,9], in the range of SC fluctuations, cuprates retain the finite value of superfluid density n_s (T), and the FCPs behave mainly as SC Cooper pairs, but without long-range order (known as "short-range phase correlations") that is confirmed by a number of experiments[66,70,71]. This result once again underlines a noticeable difference in the behavior of YBCO single crystals with and without defects.

T_{01} also determines d_{01} (distance between the conducting CuO_2 planes). In this case, regardless of the density of charge carriers, $d_{01} \sim 3.5$ Å, in agreement with the determinations of structural studies[50]. This result, together with the presence of the fluctuation contribution of 2D-MT in FLC, confirms the good structure of the samples. It should be also noted that with increasing T_c, $\xi_c(0)$, as it was found, decreases from 0.86 Å (A1) to 0.81 Å (A3) (Table 1), that is $\xi \sim 1/T_c$. The result is fully consistent with the theory of superconductivity, where $\xi \sim \hbar \nu_F / \pi k_B T_c$[26], because, as well as in the well-structured YBCO films[20], ν_F is almost independent on n_f (Table 3).

Having determined the parameters of the FLC analysis, the physical meaning of the short coherence length $\xi_{ab}(0)$ in HTSCs was examined in the framework of the simple two-dimensional model of free charge carriers[52–54]. This approach allowed us to define a set of additional important parameters of the samples, including τ_φ, which is actually the FCPs lifetime in the range SC fluctuations. Most of the calculated parameters are in good agreement with similar data obtained for OD YBCO[20,52–54,58,59]. It is shown that found $\tau_\varphi(100$ K$) = (4.49 \pm 0.06) \, 10^{-13}$ s (Table 3) is only slightly (~1.2 times) more than in well-structured YBCO films, but, as in films, in fact does not depend on n_f. Accordingly, $\tau_\varphi(100$ K$)/\tau(100$ K$) \sim 4$ is in excellent agreement with the Bieri-Maki-Thompson theory, which takes into account the approximation of the clean limit $(l > \xi)$[41], which always takes place in HTSCs due to the small value of $\xi(T)$. A certain role in this may be played by the presence of structural and kinematic anisotropy in the system[72–75].

The PG analysis has shown that the $\Delta^*(T)$ curves (Fig. 6) have the shape characteristic of YBCO films[12,54], with a clear maximum at $T = T_{pair} \approx 124$ K and a minimum at $T \approx T_{01}$[31,41]. According to the theory of systems with low n_f[8,9,27–30], T_{pair} separates both BEC and BCS regimes of LPs formation[8–12,27–29]. In full accordance with the PD of cuprates, $\Delta^*_{max}(T_{pair})/k_B$ expectedly increases from 258 K (A1) to 270 K (A3) along with an increase in n_f and T_c (Fig. 6). The BCS ratio $D^* = 2\Delta^*(T_G)/k_B T_c$ also increases from 5.0 to 5.3, suggesting the expected increase in bonding energy of the LPs[11,27,30]. At the same time, T_{pair} practically does not change (Table 3), which is understandable due to the high T_c of the samples. When approaching T_c, the PG curves show behavior being typical for all HTSCs with a maximum $\Delta^*(T)$ just below T_0 and a minimum value at $T = T_G$ (inset in Fig. 6). Thus, the approach within the LP model makes it possible to determine the exact values of T_G and, as a consequence, to obtain reliable values of $\Delta^*(T_G) \approx \Delta(0)$[12,54,65–67] (Table 4).

Finally, the shape of the $\Delta^*(T)$ curves near T_c (Fig. 6), was found to be very similar to the temperature dependence of the density of LPs in HTSCs $<n_\uparrow n_\downarrow>$ calculated within the three-dimensional attractive Hubbard model for different values of temperature, interaction, and filling factors (the Peters-Bauer model (PB)[6]). For the first time, an estimation of the density of local pairs $<n_\uparrow n_\downarrow>$ in the optimally doped YBCO was carried out by comparing the experimental data of $\Delta^*(T)$ with the PB theory (Fig. 7). It was determined that $<n_\uparrow n_\downarrow> \approx 0.3$ near T_c, which, likely, is a typical value for HTSCs.

Experimental methods. The YBa$_2$Cu$_3$O$_{7-\delta}$ single crystals were grown by the solution-melt technology in a gold crucible, according to the procedure described in[76,77]. As is well known, with an increase in the oxygen content a tetra-ortho structural transition occurs in YBa$_2$Cu$_3$O$_{7-\delta}$[78], which leads to a twinning of the single crystal and the creation of twin boundaries (TB), minimizing its elastic energy[76]. To obtain an untwined sample, the crystal was untwined into a special cell at a temperature 420 °C and a pressure 30–40 GPa, according to the procedure proposed previously[79]. In order to obtain the uniform controlled oxygen content, the crystal after untwined was repeatedly annealed for seven days in an oxygen atmosphere at 420 °C[80].

Rectangular crystals of about $1.7 \times 1.2 \times 0.2$ mm were selected from the same batch to perform the resistivity measurements. The smallest parameter of the crystal corresponds to the c-axis. The experimental geometry was selected so that the transport current vector was parallel to the ab-plane. The four-point probe technique with stabilized measuring current of up to 10 mA was used to measure the ab-plane resistivity, $\rho_{ab}(T)$ [40, and references therein]. Silver epoxy contacts were glued to the extremities of the crystal in order to produce a uniform current distribution in the central region where voltage probes in the form of parallel stripes were placed. The procedure for making contacts was completed by adding silver wires with a diameter of 0.05 mm and a three-hour annealing at a temperature of 200 °C in an oxygen atmosphere. Contact resistances below 1 Ω were obtained. The temperature was measured using a Pt sensor having an accuracy of about 1 mK. The measurements were carried out in the temperature drift mode on two opposite directions of the transport current to eliminate the influence of the parasitic signal. The critical temperature, T_c, was determined by extrapolation of the linear part of the SC transition to its intersection with the axis T[4,5,20,21].

In order to change the oxygen content and, and obtain the appropriate values of n_f and T_c, the sample was annealed for two days in an oxygen flow at temperature 620 °C. After annealing, the crystal was cooled to room temperature within 2–3 minutes, mounted in a measuring cell, and cooled to the temperature of liquid nitrogen for 10–15 minutes (sample A1). All measurements were carried out by heating the sample. To study the effect of annealing at room temperature, the sample after the first measurements of $\rho(T)$ was kept for 20 hours at room temperature (sample A2) and then repeated measurements were performed. The following measurements were carried out after additional exposure of the sample at room temperature for three days (sample A3). After this procedure, not only increased T_c and decreased $\rho(T)$, but unlike the data of the previous work[7], the PG temperature T* also decreased noticeably, whereas the value of PG increased, which is in full agreement with the PD for YBCO (refer to[3–5,13,21] and references therein).

References

1. Mishra, V., Chatterjee, U., Campuzano, J. C. & Norman, M. R. Effect of the pseudogap on the transition temperature in the cuprates and implications for its origin. *Nat. Phys.* **10**, 357–360 (2014).
2. Taillefer, L. Scattering and Pairing in Cuprate Superconductors. *Annu. Rev. Condens. Matter Phys.* **1**, 51–70 (2010).
3. Badoux, S. *et al.* Change of carrier density at the pseudogap critical point of a cuprate superconductor. *Nature (London)* **531**, 210–214 (2016).
4. Alloul, H., Rullier-Albenque, F., Vignolle, B., Colson, D. & Forget, A. Superconducting fluctuations, pseudogap and phase diagram in cuprates. *EPL* **91**, 37005 (2010).
5. Rullier-Albenque, F., Alloul, H. & Rikken, G. High-field studies of superconducting fluctuations in high-T$_c$ cuprates: Evidence for a small gap distinct from the large pseudogap. *Phys. Rev. B* **84**, 014522 (2011).
6. Peters, R. & Bauer, J. Local origin of the pseudogap in the attractive Hubbard model. *Phys. Rev. B* **92**, 014511 (2015).
7. Vovk, R. V., Vovk, N. R., Samoilov, A. V., Goulatis, I. L. & Chroneos, A. Effect of long aging on the resistivity properties of optimally doped YBa$_2$Cu$_3$O$_{7-\delta}$ single crystals. *Solid State Commun.* **170**, 6–9 (2013).
8. Emery, V. J. & Kivelson, S. A. Importance of phase fluctuations in superconductors with small superfluid density. *Nature (London)* **374**, 434–437 (1995).
9. Randeria, M. Ultracold Fermi gases: Pre-pairing for condensation. *Nat. Phys.* **6**, 561–562 (2010).
10. Grbić, M. S. *et al.* Temperature range of superconducting fluctuations above T$_c$ in YBa$_2$Cu$_3$O$_{7-\delta}$ single crystals. *Phys. Rev. B* **83**, 144508 (2011).
11. Solovjov, A. L. Pseudogap and local pairs in high-T$_c$ superconductors, *Superconductors – Materials, Properties and Applications*, Ed. A. M. Gabovich (InTech. Rijeka) Chap. 7, p. 137–170 (2012).
12. Solovjov, A. L. & Dmitriev, V. M. Resistive studies of the pseudogap in YBCO films with consideration of the transition from BCS to Bose–Einstein condensation. *Low Temp. Phys.* **32**, 99–108 (2006).
13. Ando, Y. *et al.* Electronic phase diagram of high-T$_c$ cuprate superconductors from a mapping of the in-plane resistivity curvature. *Phys. Rev. Lett.* **93**, 267001 (2004).
14. Stojkovic, B. P. & Pines, D. Theory of the longitudinal and Hall conductivities of the cuprate superconductors. *Phys. Rev. B* **55**, 8576–8595 (1997).
15. Timusk, T. & Statt, B. The pseudogap in high-temperature superconductors: an experimental survey. *Rep. Prog. Phys.* **62**, 161–214 (1999).
16. Alloul, H., Ohno, T. & Mendels, P. ^{89}Y NMR evidence for a fermi-liquid behavior in YBa$_2$Cu$_3$O$_{6+x}$. *Phys. Rev. Lett.* **63**, 1700–1703 (1989).
17. Kondo, T. *et al.* Formation of Gapless Fermi Arcs and Fingerprints of Order in the Pseudogap State of Cuprate Superconductors. *Phys. Rev. Lett.* **111**, 157003 (2013).
18. Kordyuk, A. A. Pseudogap from ARPES experiment: three gaps in cuprates and topological superconductivity. *Low Temp. Phys.* **41**, 417–444 (2015).
19. Peng, Y. Y. *et al.* Re-entrant charge order in overdoped (Bi,Pb)$_{2.12}$Sr$_{1.88}$CuO$_{6+\delta}$ outside the pseudogap regime. *Nature Materials.* **17**, 697–702 (2018).
20. Solovjov, A. L., Habermeier, H.-U. & Haage, T. Fluctuation conductivity in YBa$_2$Cu$_3$O$_{7-y}$ films of various oxygen content. II. YBCO films with T$_c \gg 80$ K. *Low Temp. Phys.* **28**, 144–156 (2002).
21. Vovk, R. V. & Solovjov, A. L. Electric transport and pseudogap in high-temperature superconducting compounds of system 1-2-3 under conditions of all-round compression. *Low Temp. Phys.* **44**, 111–153 (2018).
22. Herbut, I. F. Antiferromagnetism from Phase Disordering of a d-Wave Superconductor. *Phys. Rev. Lett.* **88**, 047006 (2002).
23. Anderson, P. W. *et al.* The physics behind high-temperature superconducting cuprates: the 'plain vanilla' version of RVB. *Phys. Cond. Mater.* **16**, R755–R759 (2004).
24. Aslamazov, L. G. & Larkin, A. L. The influence of fluctuation pairing of electrons on the conductivity of the normal metal. *Phys. Lett. A* **26**, 238–239 (1968).

25. Hikami, S. & Larkin, A. I. Magnetoresistance of high temperature superconductors. *Mod. Phys. Lett. B* **2**, 693–698 (1988).
26. De Gennes, P. G. *Superconductivity of Metals and Alloys* (W. A. Benjamin, Inc., New York, Amsterdam) **280** (1968).
27. Haussmann, R. Properties of a Fermi liquid at the superfluid transition in the crossover region between BCS superconductivity and Bose-Einstein condensation. *Phys. Rev. B* **49**, 12975–12983 (1994).
28. Loktev, V. M. Peculiarities of superconductivity in 2D metals: transition from Cooper pairing to local pairing. *Low Temp. Phys.* **22**, 490–493 (1996).
29. Tchernyshyov, O. Non-interacting Cooper pairs inside a pseudogap. *Phys. Rev. B* **56**, 3372–3400 (1997).
30. Engelbrecht, J. R., Nazarenko, A., Randeria, M. & Dagotto, E. Pseudogap above T_c in a model with d_{x2-y2} pairing. *Phys. Rev. B* **57**, 13406–13409 (1998).
31. Solovjov, A. L. *et al.* Specific temperature dependence of pseudogap in $YBa_2Cu_3O_{7-\delta}$ nanolayers. *Phys. Rev. B* **94**, 224505 (2016).
32. Dzhumanov, S. *et al.* Temperature-independent pseudogap and thermally activated c-axis hopping conductivity in layered cuprate superconductors. *Superlattices and Microstructures (Elsevier)* **68**, 6–15 (2014).
33. Habermeier, H.-U. Pulsed laser deposition - a versatile technique only for high-temperature superconductor thin-film deposition? *Appl. Surf. Sci.* **69**, 204–211 (1993).
34. Vovk, R. V. *et al.* Resistive investigation of pseudogap state in non-stoichiometric $ReBa_2Cu_3O_{7-\delta}$ (Re = Y, Ho) single crystals with due account for BCS - BEC crossover. *J. Alloys Compd.* **485**, 121–123 (2009).
35. Vovk, R. V. *et al.* Effect of small oxygen deficiency on the para-coherent transition and 2D–3D crossover in untwinned $YBa_2Cu_3O_{7-\delta}$ single crystals. *J. Alloys Compd.* **509**, 4553–4556 (2011).
36. Su, H., Welch, D. O. & Wong-Ng, W. Strain effects on point defects and chain-oxygen order-disorder transition in 123 cuprate compounds. *Phys Rev B* **70**, 054517 (2004).
37. Varotsos, P. Calculation of point defect parameters in diamond. *Phys Rev B* **75**, 172107 (2007).
38. Varotsos, P. Point defect parameters in β-PbF2 revisited. *Solid State Ionics* **179**, 438–441 (2008).
39. L. de Mello, E. V. *et al.* Pressure studies on the pseudogap and critical temperatures of a high-T_c superconductor. *Phys. Rev. B* **66**, 092504 (2002).
40. Solovjov, A. L., Tkachenko, M. A., Vovk, R. V. & Chroneos, A. Fluctuation conductivity and pseudogap in HoBaCuO single crystals under pressure with transport current flowing under an angle 45° to the twin boundaries. *Physica C* **501**, 24–31 (2014).
41. Solovjov, A. L. *et al.* Peculiarities in the pseudogap behavior in optimally doped $YBa_2Cu_3O_{7-\delta}$ single crystals under pressure up to 1 GPa. *Curr. Appl. Phys.* **16**, 931–938 (2016).
42. Solovjov, A. L. Fluctuation conductivity in Y-Ba-Cu-O films with artificially produced defects. *Low Temp. Phys.* **28**, 1138–1149 (2002).
43. Lang, W., Heine, G., Schwab, P., Wang, X. Z. & Bauerle, D. Paraconductivity and excess Hall effect in epitaxial $YBa_2Cu_3O_7$ films induced by superconducting fluctuations. *Phys. Rev. B* **49**, 4209–4217 (1994).
44. Lawrence, W. E. & Doniach, S. *Proc. of the Twelfth Int. Conf. on Low Temp. Phys.*, Kyoto, Japan (1970), E. Kanda (ed.), Keigaku: Tokyo, **361** (1970).
45. Bieri, J. B., Maki, K. & Thompson, R. S. Nonlocal effect in magnetoconductivity of high-T_c superconductors. *Phys. Rev. B* **44**, 4709–4711 (1991).
46. Xie, Y. B. Superconducting fluctuations in the high-temperature superconductors: Theory of the dc resistivity in the normal state. *Phys. Rev. B* **46**, 13997–14000 (1992).
47. Vovk, R. V. *et al.* Effect of praseodymium on the electrical resistance of $YBa_2Cu_3O_{7-\delta}$ single crystals. *Solid State Commun.* **190**, 18–22 (2014).
48. Vovk, R. V. *et al.* Effect of high pressure on the fluctuation paraconductivity in $Y_{0.95}Pr_{0.05}Ba_2Cu_3O_{7-\delta}$ single crystals. *Curr. Appl. Phys.* **14**, 1779–1782 (2014).
49. Vovk, R. V. *et al.* Resistive measurements of the pseudogap in lightly Pr-doped $Y_{1-x}Pr_xBa_2Cu_3O_{7-\delta}$ single crystals under high hydrostatic pressure. *Solid State Commun.* **204**, 64–66 (2015).
50. Chryssikos, G. D. *et al.* X-ray diffraction and infrared investigation of $RBa_2Cu_3O_7$ and $R_{0.5}Pr_{0.5}Ba_2Cu_3O_7$ compounds (R, Y and lanthanides). *Physica C* **254**, 44–62 (1995).
51. Oh, B. *et al.* Upper critical field, fluctuation conductivity, and dimensionality of $YBa_2Cu_3O_{7-x}$. *Phys. Rev. B* **37**, 7861 (1988).
52. Matsuda, Y. *et al.* Magnetoresistance of c-axis-oriented epitaxial $YBa_2Cu_3O_{7-x}$ films above T_c. *Phys. Rev. B* **40**, 5176–5179 (1989).
53. Sugawara, J. *et al.* Fluctuation conductivity of a c-axis-oriented $YBa_2Cu_3O_y$ film prepared by chemical vapor deposition. *Phys. Rev. B* **46**, 14818–14822 (1992).
54. Solovjov, A. L. & Dmitriev, V. M. Fluctuation conductivity and pseudogap in high-temperature YBCO superconductors. *Low Temp. Phys.* **35**, 227–264 (2009).
55. Sze, S. M. Physics of Semiconductor Devices. *New York: Wiley-Intercience*, **328** (1969).
56. Dzhumanov, S. & Kurbanov, U. The coexisting of insulating and metallic/superconducting phases and their competing effects in various underdoped cuprates, *Modern Physics Letters B*, 1850312–1850322 (2018).
57. Pashitskii, E. A. Low frequency charge density excitations and high-Tc superconductivity in cuprate metal-oxide compounds. I. The HTSC problem prior to a discovery of the high-Xc superconductors: predictions and premises.; Low frequency charge density excitations and high-rc superconductivity in cuprate metal-oxide compounds. II. The HTSC problem after discovery of high-temperature supercon ductors: achievements and outlooks *Low Temp. Phys.* **21**, 995–1019, 1091–1137 (1995).
58. Semba, R. & Matsuda, A. Vanishingly small Maki-Thompson superconducting fluctuation in the magnetoresistance of high-T_c superconductors. *Phys. Rev. B* **55**, 11103–11106 (1997).
59. Balestrino, G. M. *et al.* Excess conductivity in 2:2:1:2-phase Bi-Sr-Ca-Cu-O epitaxial thin films. *Phys. Rev. B* **46**, 14919–14921 (1992).
60. Segawa, K. & Ando, Y. Intrinsic Hall response of the CuO_2 planes in a chain-plane composite system of $YBa_2Cu_3O_y$. *Phys. Rev. B* **69**, 104521 (2004).
61. Wang, K. W. & Ching, W. Y. A structural-based microscopic theory on high-temperature cuprate superconductors. *Physica C* **416**, 47–67 (2004).
62. Zaitsev, R. O. Equations of two-fluid hydrodynamics in the Hubbard model. *JETP* **110**, 594–603 (2010).
63. Volz, W. *et al.* Magnetoresistance and the effect of superconducting fluctuationsin $YBa_2Cu_3O_7/PrBa_2Cu_3O_7$ superlattices. *Phys. Rev. B* **55**, 6631–6635 (1997).
64. Kondo, T. *et al.* Disentangling Cooper-pair formation above the transition temperature from the pseudogap state in the cuprates. *Nat. Phys.* **7**, 21–25 (2011).
65. Leridon, B. *et al.* Conductivity of Underdoped $YBa_2Cu_3O_{7-\delta}$: Evidence for Incoherent Pair Correlations in the Pseudogap Regime. *Phys. Rev. Lett.* **87**, 197007 (2001).
66. Yamada, Y. *et al.* Interlayer tunneling spectroscopy and doping-dependent energy-gap structure of the trilayer superconductor $Bi_2Sr_2Ca_2Cu_3O_{10+\delta}$. *Phys. Rev. B* **68**, 054533 (2003).
67. Stajic, E. *et al.* Cuprate pseudogap: Competing order parameters or precursor superconductivity. *Phys. Rev. B* **68**, 024520–024529 (2003).
68. Prokof'ev, D. D., Volkov, M. P. & Bojkov, Y. A. Pseudogap and its temperature dependence in YBCO from the data of resistance measurements. *Phys. Solid State* **45**, 1223–1232 (2003).
69. Solovjov, A. L. Fluctuating Cooper pairs in FeSe at temperatures twice above T_c (unpublished).
70. Corson, J. *et al.* Vanishing of phase coherence in underdoped $Bi_2Sr_2CaCu_2O_{8+\delta}$. *Nature* **398**, 221–223 (1999).

71. Kawabata, K. *et al*. Detection of a coherent boson current in the normal state of a high-temperature superconductor YBa$_2$Cu$_3$O$_y$ film patterned to micrometer-sized rings. *Phys. Rev. B* **58**, 2458–2461 (1998).
72. Downing, C. A. & Portnoi, M. E. Bielectron vortices in two-dimensional Dirac semimetals. *Nature Commun.* **8**, 897–902 (2017).
73. Dobrovolskiy, O. V. *et al*. Mobile fluxons as coherent probes of periodic pinning in superconductors. *Sci. Rep.* **7**, 13740 (2017).
74. Curran, P. G. *et al*. Vortex imaging and vortex lattice transitions in superconducting Sr$_2$RuO$_4$ single crystals. *Phys. Rev. B* **84**, 104507 (2011).
75. Adamenko, I. N. & Nemchenko, E. Diffusion of quasi-particles of 3He- 4He mixtures and classical particles. *Low Temp. Phys.* **21**, 498–508 (1995).
76. Vovk, R. V., Khadzhai, G. Y. & Dobrovolskiy, O. V. Transverse conductivity in Pr$_y$Y$_{1-y}$Ba$_2$Cu$_3$O$_{7-\delta}$ single crystals in a wide range of praseodymium concentrations. *Appl. Phys. A* **117**, 997–1002 (2014).
77. Widder, K. *et al*. Ordering of chain oxygen in YBa$_2$Cu$_3$O$_x$.Optical investigations on single-domain crystals. *Physica C* **232**, 82–88 (1994).
78. Cava, R. J. Structural chemistry and the local charge picture of copper oxide superconductors. *Science* **247**, 656–662 (1990).
79. Giapintzakis, J., Ginzberg, D. M. & Han, P. D. A method for obtaining single domain superconducting YBa$_2$Cu$_3$O$_{7-x}$ single crystals. *J. Low Temp. Phys.* **77**, 155–161 (1989).
80. Vovk, R. V. *et al*. Effect of redistribution of labile oxygen on the pseudogap state in untwinned YBa$_2$Cu$_3$O$_{7-x}$ single crystals. *Low Temp. Phys.* **33**, 931–934 (2007).

Author Contributions

Additional Information